Published in final edited form as:
Cancer Res. 2012 June 1; 72(11): 2738–2745. doi:10.1158/0008-5472.CAN-11-4027.

In vivo diagnosis of melanoma and non-melanoma skin cancer using oblique incidence diffuse reflectance spectrometry

Alejandro Garcia-Uribe[1,2], **Jun Zou**[2], **Madeleine Duvic**[3], **Jeong Hee Cho-Vega**[4], **Victor G. Prieto**[4], and **Lihong V. Wang**[1,*]

[1]Department of Biomedical Engineering, Washington University in St. Louis, St. Louis, MO 63130

[2]Department of Electrical and Computer Engineering, Texas A&M University, College Station, TX 77843

[3]Department of Dermatology, the University of Texas M. D. Anderson Cancer Center, Houston, TX 77030

[4]Department of Pathology, the University of Texas M. D. Anderson Cancer Center, Houston, TX 77030

Abstract

Early detection and treatment of skin cancer can significantly improve patient outcome. However, present standards for diagnosis require biopsy and histopathologic examinations that is relatively invasive, expensive and difficult for patients with many early stage lesions. Here we show an oblique incidence diffuse reflectance spectroscopic (OIDRS) system that can be used for rapid skin cancer detection in vivo. This system was tested under clinical conditions by obtaining spectra from pigmented and non-pigmented skin lesions, including melanomas, differently staged dysplastic nevi and common nevi that were validated by standard patho-histological criteria. For diagnosis of pigmented melanoma, the data obtained achieved 90% sensitivity and specificity for a blinded test set. In a second analysis, we demonstrated that this spectroscopy system can also differentiate non-pigmented basal cell or squamous cell carcinomas from non-cancerous skin abnormalities such as actinic keratoses and seborrheic keratoses, achieving 92% sensitivity and specificity. Taken together, our findings establish how oblique incidence diffuse reflectance spectrometry can be used to more rapidly and easily diagnose skin cancer in an accurate and automated manner in the clinic.

1. Introduction

Skin cancer is the most common form of cancer, with about a million new cases in the U.S. each year [1]. Often, skin cancer is difficult to diagnose non-invasively, as malignant skin lesions can closely resemble their benign counterparts. Different lesion types can have similar characteristics, furthering the problem in discriminating among them. Among all the skin lesions, melanoma is the most malignant type and is the leading cause of death from the skin diseases.

The American Cancer Society estimates that there will be approximately 62,000 new cases of melanoma in the U.S. this year, with about 8,000 deaths [1]. Melanoma can be mistaken for common nevi, dysplastic nevi, and seborrheic keratoses (SK). Common nevi are benign moles formed by a cluster of melanocytes in the basal layer of the epidermis or in the top layers of the dermis. Dysplastic nevi are moles with atypical size, shape, or organization.

*Corresponding author: lhwang@wustl.edu. .

Depending on the degrees of atypia, dysplastic nevi can be mild, moderate, or severe. Dysplastic nevi are more likely than common nevi to develop into melanomas [2]. Finally, seborrheic keratoses (SK) are benign wart-like tumors that are very common in people over forty.

In addition to melanoma, skin cancers also include squamous cell carcinomas and basal cell carcinomas. Squamous cell carcinomas (SCC) arise from dividing keratinocytes of the epidermis, and are often recognized by hyperkeratotic crusts or scales or by ulceration in the later stages. Actinic keratosis (AK), a precancerous skin tumor caused by sun exposure, can in some cases turn into squamous cell carcinoma, which in invasive cases may metastasize to local nodes and beyond [3]. Basal cell carcinomas (BCC) are derived from keratinocytes [4]. BCCs are locally invasive, slow-growing tumors characterized by islands or nests of basal keratinocytes invading the dermis. There are several clinical and histologic subtypes of basal cell carcinomas. Superficial BCCs are papulosquamous lesions characterized by red, scaly raised plaques.

Early detection and treatment of skin cancer can significantly improve patient outcomes. In clinical practice, visual examination determines whether a skin lesion is cancerous based on the ABCDE rule (asymmetry, border, color, diameter and evolution) and the change in the appearance of a mole or pigmented area over a period of time. However, clinical diagnostic sensitivity and specificity vary greatly, depending on the expertise and visual skills of the clinician. Consequently, histopathologic examination of the excised suspicious element still remains the gold standard. However, biopsy is an invasive procedure and leaves a scar at the biopsy site, which otherwise would be unnecessary in the case of benign lesions. Moreover, the removal of every lesion can be unacceptable for patients with large numbers of skin abnormalities, such as in dysplastic nevi syndrome.

Changes in the cell nuclear matrix have been associated with cell and tissue structures which are important features in the diagnosis of cancer [5,6]. Morphological changes in tumor cells include alterations of nuclear structure such as changes in nuclear size and shape [5]. These alterations are important characteristics used in cancer diagnosis. Cell nuclei, mitochondria, other cytoplasmic organelles and cell nuclei, are the major light scatterers in the skin tissue. In malignant tissues, larger atypical nuclei and larger cell volume are a main cause for the significant increase in the light scattering [7]. For example, the reduced scattering coefficient has been shown to generally increase with the degree of dysplasia or malignancy of skin lesions [8].

Recently, non-invasive spectroscopic methods for tissue diagnosis have been studied for a number of organ systems, including the skin [9-19], gastrointestinal tract [20-24], cervix [25-27], and breast [28-30]. The absorption of light can provide information of the biochemical composition of the skin. The light scattering properties of skin can provide information regarding its micro-architecture [31]. Fluorescence spectroscopy can detect disease states [32,33]. Because fluorescence is a manifestation of the biochemical environment of the cell, it should be a specific indicator of cellular alterations due to disease [34]. Some studies also suggest that Raman spectroscopy can detect changes in protein and lipid structure that can be used to diagnose skin tumors [35]. In this paper, we report the use of spatially resolved oblique incidence diffused reflectance spectroscopy (OIDRS) as a non-invasive tool to discriminate melanoma and non-melanoma skin cancer from benign and premalignant skin lesions *in vivo*. Spatio-spectral diffuse reflectance data within the wavelength range of 455–765 nm was collected from multiple types of pigmented and non-pigmented skin lesions ($n = 678$). The data was used in combination with artificial neural network (ANN) analysis to separate skin cancers such as pigmented malignant melanoma and non-pigmented basal cell and squamous cell carcinomas from their benign counterparts.

Neural networks are particularly helpful for classification. ANN classifiers are more powerful than common statistical classifiers because they do not need hypothesis about data distribution, linearity or correlations [36]. ANNs provide better prediction accuracy and higher sensitivity and specificity with optimal use of the available information.

2. Methods

Fig. 1 is a schematic of the experimental OIDRS system. The system was built onto a portable cart; it was easily moved to the patient exam rooms. To target both small and large skin lesions, we constructed an optical fiber probe using micromachining technology. The probe consisted of three source fibers and two linear arrays of 12 collection fibers within an area of 2×2 mm^2. To conduct OIDRS measurements on skin lesions, the optical probe was placed gently on the skin area of interest without significant compression. The optical multiplexer delivered light through only one oblique source fiber at a time to the area of interest. Once the light was delivered to the skin, it interacted with the skin tissue, and the spatially resolved diffuse reflectance was collected by one set of collection fibers. The collection fibers were coupled to an imaging spectrograph that generated an optical spectrum from 455 to 765 nm for the collection channel. A CCD camera collected the spectral images, which were stored on a computer for data analysis. The data collection takes less than 5 minutes, and it did not interfere with the standard healthcare provided to the patients.

Data was collected at the University of Texas M.D. Anderson Cancer Center in Houston, TX. A physician identified the lesion(s) to be measured before the scheduled biopsy. To average out the effect of structural anisotropy of the skin tissue, the measurement of each lesion was repeated four times to obtain images from different orientations. To provide self-references, the same measurements were also repeated on the neighboring healthy skin tissues. The anisotropy is defined as the variation of the measurements when performed in different directions. After the measurements were completed, a biopsy was performed for each skin lesion and submitted for histopathological analysis. The histopathological analysis determined that the measured pigmented lesions consisted of benign common nevi (CN), mildly dysplastic nevi (DN1), moderately dysplastic nevi (DN2), severely dysplastic nevi (DN3), and melanomas (M). The criteria used to divide dysplastic nevi into these tree categories is described in ref. [37]. Of the 407 pigmented skin lesions, 271 were used for the training sets of ANN classifiers (Tables I and II) to separate malignant melanoma from varieties of nevi. The remaining 136 data sets were used to test the efficacy of the ANN classifiers. The non-pigmented lesions consisted of basal cell carcinomas (BCC), squamous cell carcinomas (SCC), benign actinic keratoses (AK), and seborrheic keratoses (SK). Among the 266 non-pigmented lesions, 177 were used to train the ANN classifier, and the remaining 89 were used for testing.

3. Results

The absorption coefficient (μ_a) and reduced scattering coefficient (μ_s') of the skin lesions from the measured diffuse reflectance were estimated based on a combination of both diffusion theory and scalable Monte Carlo simulation [38,39]. Since the optical transport mean free path (L_t') is a function of the wavelength of the incident light, the location of the detectors may fall either within or outside the range of L_t' at different wavelengths within the wide spectrum (455 – 765 nm). At certain wavelengths, when the location of the detectors falls outside the range of L_t', the absorption and scattering optical properties of the skin lesion can be directly calculated from diffuse reflectance using a straightforward diffusion-theory based analytical model. However, this model would fail at other wavelengths when the detector location falls within L_t'. In this case, scalable Monte Carlo

simulation was conducted to deduce the absorption and scattering optical properties of the skin lesions in an inverse problem by calculating and matching the simulated diffuse reflectance results with the actual measurements.

The optical properties of human skin vary significantly between locations and individuals, dependent on race, age, sun exposure, and skin type. Figs. 2a and 2b show the absorption coefficient (μ_a) for the statistically significant skin types included in this study. We reduced these variations by measuring and subtracting the optical priorities from the surrounding healthy skin for each lesion. The differential absorption coefficient spectrum is defined as

$$\Delta\mu_a(\lambda) = \mu_a(\lambda)_L - \mu_a(\lambda)_N \quad (1)$$

where $\mu_a(\lambda)_L$ and $\mu_a(\lambda)_N$ are the absorption coefficient spectra measured from the lesion and from the normal surrounding skin, respectively. In a similar way the differential reduced scattering coefficient is defined as

$$\Delta\mu_s'(\lambda) = \mu_s'(\lambda)_L - \mu_s'(\lambda)_N \quad (2)$$

Fig. 2 shows the average absorption coefficient $\mu_a(\lambda)_L$, differential absorption coefficient $\Delta\mu_a(\lambda)$, reduced scattering coefficient $\mu_s'(\lambda)_L$, and differential reduced scattering coefficient $\Delta\mu_s'(\lambda)$ for melanoma, dysplastic nevi and common nevi, respectively.

The diffuse reflectance of tissue is related largely to absorption and scattering. Mitochondria, cell nuclei, and other cytoplasmic organelles are known changeable parameters in cancerous tissues and are major light scatterers in skin tissue [40,41]. Although no single histologic variable specifically distinguishes these types of pigmented lesions, nuclear atypia seems directly related to the amount of light scattering. Dysplastic nevi are characterized by nuclear enlargement, slight irregularity, and hyperchromasia, with clumping of chromatin and sometimes with prominent nucleoli. Dysplastic nevi present atypical features that are both clinically and histologically important as simulants of melanoma. Like other cancers, most malignant melanomas evolve through a number of stages of tumor progression. Clinically, many melanomas begin as a pigmented patch of skin which evolves to become a palpable plaque, and enlarges as if it were along the radii of an imperfect circle [42]. Variably sized and shaped nests and single melanocytes are present in the epidermis in a pagetoid pattern characteristic of superficial melanoma. Prognosis has long been known to correlate with melanoma thickness as measured microscopically. These factors can increase the contribution of scattering to the diffuse reflection on the surface.

A one-way ANOVA test was performed to compare $\mu_a(\lambda)_L$ for common nevi, dysplastic nevi, and melanoma. The p-value was significant ($p<0.01$) in the spectral region between 488 and 576 nm. Pairwise comparisons using Tukey's test showed a significant difference only between common nevi and melanoma. A similar analysis for $\mu_s'(\lambda)_L$ shows a significant difference of at least one mean for the entire wavelength range (455-765 nm). The ANOVA test of the $\Delta\mu_a(\lambda)$ showed statistical difference in the range between 455 and 599 nm, with the lowest p-value at 556 nm ($p=0.00063$). The pairwise comparisons revealed that $\Delta\mu_a(\lambda)$ from 549 to 556 nm presented a significant difference among the three types of lesions. This spectral region corresponds to an absorption peak in deoxy-hemoglobin. These results showed the importance of subtracting the optical properties of the surrounding healthy skin for each lesion in order to reduce the variations due to differences in skin type and condition. The ANOVA and Tukey's tests of $\Delta\mu_s'(\lambda)$ show a significant difference among the three types of lesions when using the spectral range between 455 and 765 nm. Both squamous-cell carcinomas (SCC) and basal-cell carcinomas (BCC) presented on average a higher differential reduced scattering coefficient than actinic keratosis (AK), and

seborrheic keratosis (SK) (Fig. 3). An ANOVA and Tukey's test of $\mu_a(\lambda)_L$ revealed no significant difference among all four types of lesions. However the ANOVA test of $\Delta\mu_a(\lambda)$ showed a p-value that indicates a significant difference ($p<0.01$) in the spectral region 455–633 nm with the lowest $p=0.0008$ at 577 nm. The absorption coefficient spectra for SKs have the largest variation (Fig. 3). The subtraction of the reference absorption coefficients from the lesions' absorption coefficients reduces the overlap among the types of lesions and resulted in a statistically significant difference between AK, SCC, and BCC. The pairwise comparison of $\Delta\mu_s'(\lambda)$ between AK with SK, AK with SCC, SK with BCC, and SK with SCC in the wavelength range between 455 and 765 nm was statistically significant.

This higher light scattering in cancerous cases can be explained by the larger average effective size of the scattering centers. SCC *in-situ* has not yet penetrated through the basement membrane of the dermoepidermal junction. SCCs typically appear as scaling plaques with sharply defined red color. Histologically, all epidermal layers may contain atypical keratinocytes. The larger amount of atypical keratinocytes in SCC can increase the light scattering in this type of skin lesion and significantly affect its contribution to diffusely reflected light on the surface. SCC may penetrate the basement membrane to become invasive. More advanced, invasive SCCs may appear clinically as hyperkeratosis and may ulcerate [43], which can affect the measurements of optical properties. To avoid this problem, we performed the measurements in areas that did not present this condition.

Actinic keratosis (AK) may appear rough and scaly and may develop into a SCC. Histologically, AKs are recognized by the presence of atypical keratinocytes in the deeper portions of the epidermis. Defective maturation of the superficial epidermal layers results in parakeratosis alternating with hyperkeratosis [43,44]. During the data collection, we avoided areas that presented hyperkeratosis. The amounts of atypical keratinocytes and collagen are factors related to the amount of light scattering in the lesion.

Basal cell carcinomas (BCC) are derived from the basal layer of keratinocytes, the deepest cell layer of the epidermis. BCCs can present nodular aggregates of basalioma cells in the dermis and exhibit peripheral palisading and retraction artifacts. Melanin can also be present in the tumor and in the surrounding stroma, as observed in pigmented basal cell carcinoma. The aggregation of basalioma cells can increase the light scattering in these types of malignant lesions. The progression of seborrheic keratosis into basal cell carcinoma and squamous cell carcinoma is rare [45,46]. However, SKs can clinically resemble SCCs, and for this reason SKs are commonly removed or biopsied for histopathologic examination [47]. SKs, composed of basaloid cells admixed with some squamoid cells, can be pigmented when some cells contain melanin transferred from neighboring melanocytes.

The classifications of the skin lesions were performed directly for the measured diffuse-reflectance spectra. The advantage of using these direct measurements is that no homogeneity assumption is required. To design the classifiers, first we selected features from the diffuse-reflectance spectra that effectively separated the malignant group from the benign group. The nature of the acquired diffuse-reflectance spectra and what they represent played a role in determining their effectiveness. The characteristics of the diffuse reflectance data indicate that particular spectral regions have higher separability among the different classes. We employed the continuous wavelet transform (CWT) to extract the most effective features in the two classes under analysis [10]. Based on the features, we investigated the use of multiple classification schemes to separate the skin lesions into clinically significant categories (benign, pre-cancerous, and cancerous) as identified by their clinical and histopathologic diagnoses. The most successful classification scheme was ANN in combination with a genetic algorithm (GA). For the pigmented and non-pigmented lesion groups, we classified the lesions into two classes at a time and repeated this for the

subgroups until we achieved the desired degree of categorization. Fig. 4 illustrates the hierarchical classification system for pigmented lesions. This particular classification scheme intrinsically emphasizes the primary importance of accurate classification of melanoma and severe dysplastic nevi. Each stage consists of a single classifier. In the first stage, melanoma is separated from the other lesions. In a similar way, in each stage the most "malignant" type lesion is separated from the remaining categories.

Tables I present the confusion matrixes for the training and testing sets, where the row headers show the ground truths from the histopathologic diagnosis and the column headers indicate the OIDRS classifications. The classification process in the testing set achieved 90% sensitivity and specificity for melanoma detection. Table II shows the sensitivity and specificity for each classifier in the hierarchical classification scheme. The minimum sensitivity is 89%, which corresponds to the classifiers that separate mild dysplastic nevi form benign common nevi. Sensitivity indicates the percentage of correctly identified positives (true positives) and specificity measures the proportion of negatives which are correctly identified.

For the non-pigmented group, a single ANN classifier separated BCC and SCC from AK and SK. The designed classifier generated a sensitivity of 97% and a specificity of 96%. Table III and V show the classification results for non-pigmented lesions. For the testing set the sensitivity ands specificity were both 92 %.

5. Conclusions

This study established that it is feasible to use oblique incidence diffuse reflectance spectroscopy (OIDRS) as a potential tool for *in vivo* discrimination of malignant cutaneous melanoma from other types of pigmented skin lesions. In a clinical trial, OIDRS distinguished malignant melanoma with 90% sensitivity and specificity for the testing set. The sensitivity and specificity for the training set were 100% and 95%, respectively. This system has also successfully classified basal cell carcinomas and squamous cell carcinomas with 92% sensitivity and specificity. The sensitivity and specificity for the training set were 97% and 96%, respectively. Light scattering events inside the skin tissues change significantly with the development stage of the skin lesion. This change in the tissue scattering properties in the diffuse reflectance spectrum forms a physiological basis for automated classification of different skin lesions based on OIDRS measurements.

Acknowledgments

The authors thank Dr. Mays, Dr. Hymens, Dr. Mansfield, and the staff from the Melanoma and Skin Center at the University of Texas M. D. Anderson Cancer Center for their help during the data collection. This project was sponsored by National Institute of Health grant R01 CA106728.

References

1. American Cancer Society website. Melanoma Skin Cancer. http://www.cancer.org
2. Williams ML, Sagebiel RW. Melanoma Risk Factors and Atypical Moles. West J Med. 1994; 160:343–35. [PubMed: 8023484]
3. Cherpelis BS, Marcusen C, Lang PG. Prognostic Factors for Metastasis in Squamous Cell Carcinoma of the Skin. Dermatol Surg. 2002; 28:268–73. [PubMed: 11896781]
4. Takata M, Saida T. Early cancers of the skin: clinical, histopathological, and molecular characteristics. Int J Clin Oncol. 2005; 10:391–97. [PubMed: 16369742]
5. Zink D, Fischer AH, Nickerson JA. Nuclear structure in cancer cells. Nat Rev Cancer. 2004; 4:677–87. [PubMed: 15343274]

6. Lelievre SA, Weaver VM, Nickerson JA, Larabell CA, et al. Tissue phenotype depends on reciprocal interactions between the extracellular matrix and the structural organization of the nucleus. Proc. Natl Acad. Sci. 1998; 95:14711–16. [PubMed: 9843954]
7. Jorgensen P, Edgington NP, Schneider BL, Rupes I, Tyers M, Futcher B. The Size of the Nucleus Increases as Yeast Cells Grow. Mol Biol Cell. 2007; 18:3523–32. [PubMed: 17596521]
8. Garcia-Uribe A, Smith EB, Zou J, Duvic M, Prieto V, Wang LV. In-vivo characterization of optical properties of pigmented skin lesions including melanoma using oblique incidence diffuse reflectance spectroscopy. J Biomed Opt. 2011; 16:020501. [PubMed: 21361657]
9. Wallace VP, Bamber JC, Crawford DC, Ott RJ, Mortimer PS. Classification of reflectance spectra from pigmented skin lesions, a comparison of multivariate discriminant analysis and artificial neural networks. Phys Med Biol. 2000; 45:2859–71. [PubMed: 11049176]
10. Garcia-Uribe A, Kehtarnavaz N, Marquez G, Prieto V, Duvic M, Wang LV. Skin Cancer Detection by Spectroscopic Oblique-Incidence Reflectometry: Classification and Physiological Origins. Appl Opt. 2004; 43:2643–2650. [PubMed: 15130003]
11. McIntosh LM, Summers R, Jackson M, Mantsch HH, et al. Towards Non-Invasive Screening of Skin Lesions by Near-Infrared Spectroscopy. J Invest Dermatol. 2001; 6:75–87.
12. Sigurdsson S, Philipsen PA, Hansen LK, Larsen J, Gniadecka M, Wulf HC. Detection of Skin Cancer by Classification of Raman Spectra. IEEE Trans Biomed Eng. 2004; 51:1784–93. [PubMed: 15490825]
13. Gniadecka M, Philipsen PA, Sigurdsson S, Wessel S, et al. Melanoma Diagnosis by Raman Spectroscopy and Neural Networks: Structure Alterations in Proteins and Lipids in Intact Cancer Tissue. J Invest Dermatol. 2004; 122:443–49. [PubMed: 15009728]
14. Lynn CJ, Saidi IS, Oelberg DG, Jacques SL. Gestational age correlates with skin reflectance in newborn infants of 24-42 weeks gestation. Biol. of the Neonate. 1993; 64:69–75.
15. Moncrieff M, Cotton S, Claridge E, Hall P. Spectrophotometric intracutaneous analysis: a new technique for imaging pigmented skin lesions. Br J Dermatol. 2002; 146:448–45. [PubMed: 11952545]
16. Wallace VP, Bamber JC, Crawford DC, Ott RJ, Mortimer PS. Classification of reflectance spectra from pigmented skin lesions, a comparison of multivariate discriminant analysis and artificial neural networks. Phys. Med. Biol. 2000; 45:2859–71. [PubMed: 11049176]
17. McIntosh LM, Summers R, Jackson M, Mantsch HH, Mansfield JR, Howlett M, Crowson AN, Toole JW. Towards non-invasive screening of skin lesions by near-infrared spectroscopy. J Invest Dermatol. 2001; 116:175–81. [PubMed: 11168814]
18. Tomatis S, Carrra M, Bono A, Bartoli C, Lualdi M, Tragni G, Colombo A, Marchesini R. Automated melanoma detection with a novel multispectral imaging system: results of a prospective study. Phys. Med. Biol. 2005; 50:1675–87. [PubMed: 15815089]
19. Arifler D, Schwarz RA, Chang SK, Richards-Kortum R. Reflectance spectroscopy for diagnosis of epithelial precancer: mmodel-based analysis of fiber-optic probe designs to resolve spectral information from epithelium and stroma. Appl Opt. 2005; 44:4291–305. [PubMed: 16045217]
20. Bargo PR, Pral SA, Goodell TT, Sleven RA, Koval G, Blair G, Jacques SL. In-vivo determination of optical properties of normal and tumor tissue with white light reflectance and an empirical light transport model during endoscopy. J Biomed Opt. 2005; 10:034018. [PubMed: 16229662]
21. Mayinger B, Horner P, Jordan M, Gerlach C. Dipl.Phys. Horbach T, Hohenberger W, Hahn EG. Endoscopic fluorescence spectroscopy in the upper GI tract for the detection of GI cancer: initial experience. Am J Gastroenterol. 2001; 96:2616–21. [PubMed: 11569684]
22. Georgakoudi I, Jacobson BC, Van Dam J, Backman V, Wallace MB, Muller MG, Zhang Q, Badizadegan K, Sun D, Thomas GA, Perelman LT, Feld MS. Fluorescence, reflectance, and light-scattering spectroscopy for evaluating dysplasia in patients with Barrett's esophagus. Gastroenterology. 2001; 120:1620–29. [PubMed: 11375944]
23. Dacosta RS, Wilson BC, Marcon NE. Light-induced fluorescence endoscopy of the gastrointestinal tract. Gastrointes. Endosc Clin North Am. 2000; 10:37–69.
24. Dacosta RS, Wilson BC, Marcon NE. New optical technologies for earlier endoscopic diagnosis premalignant gastrointestinal lesions. J Gastroenterol Hepatol. 2002; 17:S85–S104. [PubMed: 12000596]

25. Mirabal YN, Chang SK, Atkinson EN, Malpica A, et al. Reflectance spectroscopy for in-vivo detection of cervical precancer. J Biomed Opt. 2002; 7:587–594. [PubMed: 12421125]
26. Ramanujam N, Mitchell MF, Mahadevan A, Warren S, Thomsen S, Silva E, Richards-Kortum R. In-vivo diagnosis of cervical intraepithelial neoplasia using 337-nm-excited laser-induced fluorescence. Proc Natl Acad Sci. 1994; 91:10193–97. [PubMed: 7937860]
27. Nath A, Rivoire K, Chang S, West L, Cantor SB, et al. A pilot study for a screening trial of cervical fluorescence spectroscopy. Int J Gynecol Cancer. 2004; 14:1097–107. [PubMed: 15571615]
28. Johnson KS, Chicken DW, Pickard DC, Lee AC, et al. Elastic scattering spectroscopy for intraoperative determination of sentinel lymph node status in the breast. J Biomed Opt. 2004; 9:1122–28. [PubMed: 15568931]
29. Fantini S, Walker SA, Franceschini MA, Kaschke M, et al. Assessment of the size, position, and optical properties of breast tumors in-vivo by noninvasive optical methods. Appl Opt. 1998; 37:1982–89. [PubMed: 18273118]
30. Tadrous PJ, Siegel J, French PM, Shousha S, et al. Fluorescence lifetime imaging of unstained tissues: early results in human breast cancer. J Pathol. 2003; 199:309–17. [PubMed: 12579532]
31. Zonios G, Dimou A. Light scattering spectroscopy of human skin in-vivo. Opt. Express. 2009; 17:1256–67. [PubMed: 19188953]
32. Gillenwater A, Jacob R, Richards-Kortum R. Fluorescence spectroscopy: A technique with potential to improve the early detection of aerodigestive tract neoplasia. Head Neck. 1998; 20:556–562. [PubMed: 9702544]
33. Müller MG, Valdez TA, Georgakoudi I, Backman V, et al. Spectroscopic detection and evaluation of morphologic and biochemical changes in early human oral carcinoma. Cancer. 2003; 7:1681–92.
34. Richards-Kortum R, Sevick-Muraca E. Quantitative optical spectroscopy for tissue diagnosis. Annual Rev. Phys. Chem. 1996; 47:555–06. [PubMed: 8930102]
35. Gniadecka M, Philipsen PA, Sigurdsson S, Wessel S, et al. Melanoma Diagnosis by Raman Spectroscopy and Neural Networks: Structure Alterations in Proteins and Lipids in Intact Cancer Tissue. J Invest Dermatol. 2004; 122:443–49. [PubMed: 15009728]
36. Haykin AS. Neural networks expand SP's horizons. IEEE Signal Process Mag. 1996; 13:24–49.
37. Shea CR, Vollmer RT, Prieto VG. Correlating architectural disorder and cytologicatypia in clark (dysplastic) melanocytic nevi. Hum Pathol. 1999; 30:500–5. [PubMed: 10333217]
38. Wang L-H, Jacques SL. Analysis of diffusion theory and similarity relations," in Photon migration and imaging in random media and tissues. Proc. Soc. Photo-Opt. Instrum. Eng. 1993; 1888:107–16.
39. Kienle A, Patterson MS. Determination of the optical properties of turbid media from a single Monte-Carlo simulation. Phys. Med. Biol. 1996; 41:2221–27. [PubMed: 8912392]
40. Mourant JR, Freyer JP, Hielscher AH, Eick AA, Shen D, Johnson TM. Mechanisms of Light Scattering from Biological Cells Relevant to Noninvasive Optical-Tissue Diagnostics. Appl Opt. 1998; 37:3586–93. [PubMed: 18273328]
41. Mourant JR, Canpolat M, Brocker C, Esponda-Ramos O, et al. Light scattering from cells: the contribution of the nucleus and the effects of proliferative status. J Biomed Opt. 2000; 5:131–7. [PubMed: 10938776]
42. Elder, David E. Precursors to melanoma and their mimics: nevi of special sites. Mod Pathol. 2006; 19:S4–S20. [PubMed: 16446715]
43. Anwar J, Wrone DA, Kimyai-Asadi A, Alam M. The development of actinic keratosis into invasive squamous cell carcinoma: Evidence and evolving classification schemes. Clin Dermatol. 2004; 22:189–196. [PubMed: 15262304]
44. Goldberg LH, Joseph AK, Tschen JA. Proliferative actinic keratosis. Int. J Dermatol. 1994; 33:341–45. [PubMed: 8039973]
45. Mikhail GR, Mehregan AH. Basal cell carcinoma in seborrheic keratosis. J Am Acad Dermatol. 1982; 6:500–06. [PubMed: 7076904]
46. Sloan JB, Jaworsky C. Clinical misdiagnosis of squamous cell carcinoma in-situ as seborrheic keratosis. A prospective study. J Dermatol Surg Oncol. 1993; 19:413–16. [PubMed: 8496484]

47. Duque MI, Jordan JR, Fleischer AB, Williford PM, et al. Frequency of seborrheic keratosis biopsies in the United States: a benchmark of skin lesion care quality and cost effectiveness. Dermatol Surg. 2003; 29:796–801. [PubMed: 12859377]

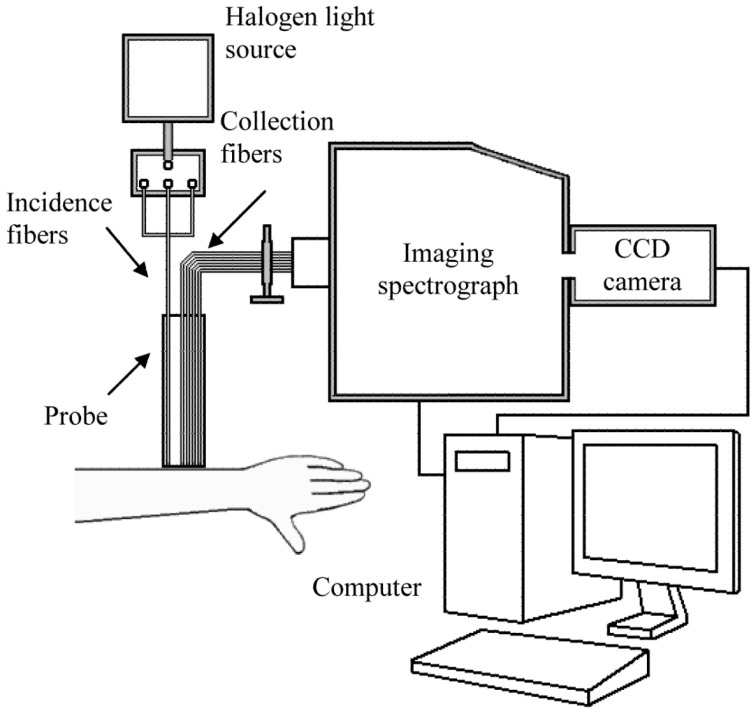

Fig. 1.
A schematic of the experimental OIDRS system.

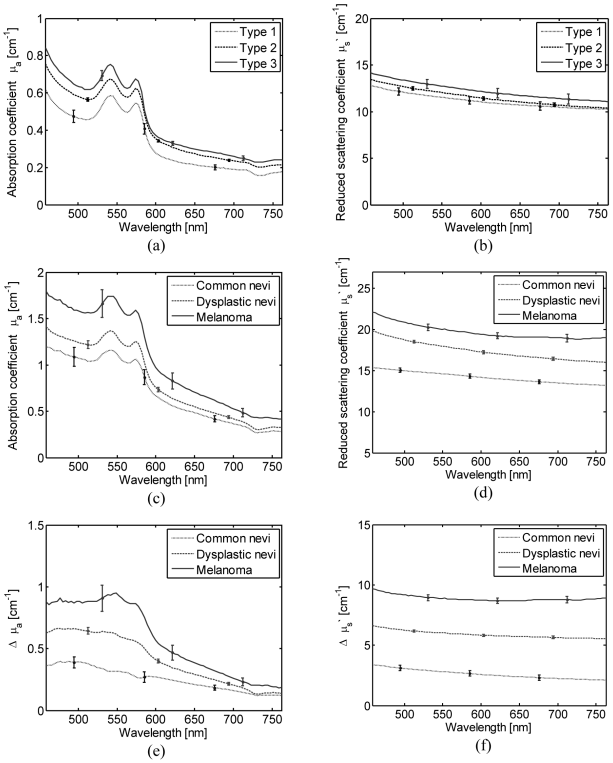

Fig. 2.

(a) Average absorption coefficient spectra $\mu_a(\lambda)$, and (b) average reduced scattering coefficient for skin types 1, 2 and 3 estimated from 47, 816, and 44 lesions, respectively, (c) Average absorption coefficient spectra, (d) average reduced scattering coefficient spectra, (e) average differential absorption coefficient spectra, and (f) average differential reduced scattering coefficient spectra for common nevi, dysplastic nevi, and melanoma. The error bars represent standard errors.

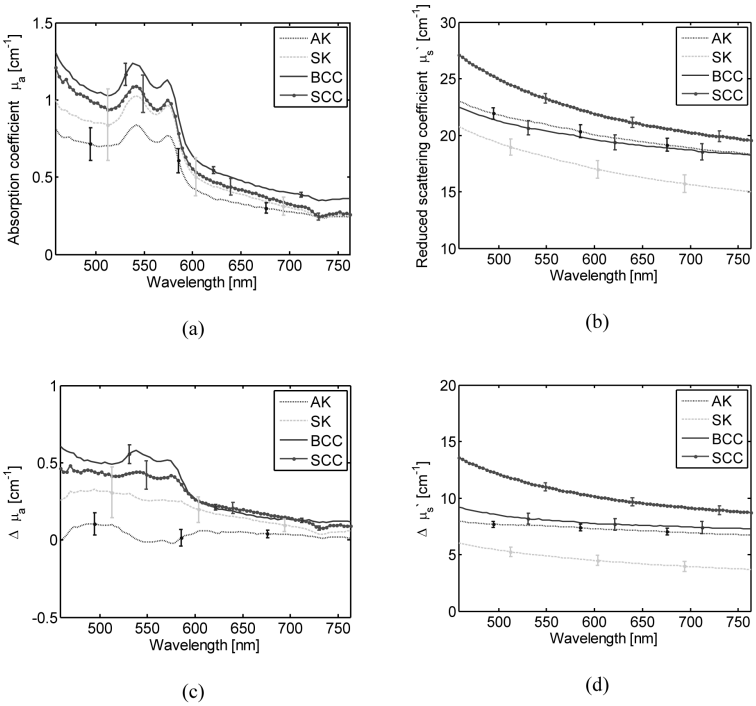

Fig. 3.

(a) Average absorption coefficient spectra, (b) average reduced scattering coefficient spectra, (c) average differential absorption coefficient spectra, and (d) average differential reduced scattering coefficient spectra for squamous-cell carcinoma (SCC), basal-cell carcinoma (SCC), actinic keratosis (AK), and seborrheic keratosis (SK). The error bars represent standard errors.

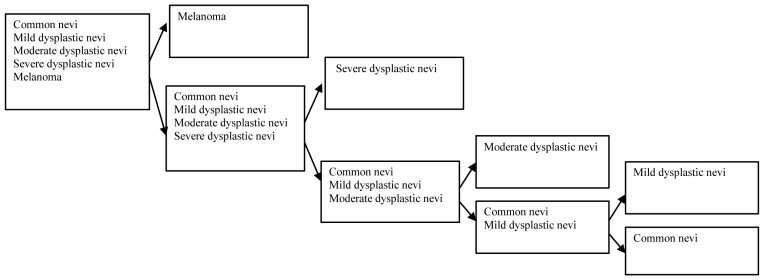

Fig. 4.
The classification scheme for pigmented lesions.

Table I

Pigmented lesions confusion matrix.

	Predicted / Actual	MM	DN3	DN2	DN1	CN	Total
Training	MM	20	0	0	0	0	20
	DN3	1	28	0	0	0	29
	DN2	4	2	118	2	1	127
	DN1	3	1	0	33	1	38
	CN	4	2	2	1	48	51
Testing	MM	9	0	1	0	0	10
	DN3	2	12	1	0	0	15
	DN2	6	2	53	2	0	63
	DN1	1	1	0	16	2	20
	CN	4	1	1	0	22	28

Table II

Sensitivity and specificity for each classifier included in the hierarchical classification scheme.

	Training		Testing		Overall	
	Sensitivity	**Specificity**	**Sensitivity**	**Specificity**	**Sensitivity**	**Specificity**
MM vs. (DN3 DN2, DN1, CN)	100 %	95 %	90 %	90 %	97 %	93 %
DN3 vs. (DN2, DN1, CN)	100 %	98 %	92 %	96 %	98 %	97 %
DN2 vs. (DN1, CN)	98 %	98 %	96 %	98 %	97 %	98 %
DN1 vs. CN	97 %	98 %	89 %	100 %	94 %	99 %

Table III

Non-pigmented lesions confusion matrix.

	Predicted Actual	BCC/SCC	AK/SK	Total
Training	BCC (n=78) /SCC (n=49)	123	4	127
	AK (n=38)/SK (n=12)	2	48	50
Testing	BCC (n=39)/SCC (n=25)	59	5	64
	AK (n=19)/SK (n=6)	2	23	25